Available online at www.sciencedirect.com
SCIENCE DIRECT®
Biochemical and Biophysical Research Communications 336 (2005) 346–356
BBRC
www.elsevier.com/locate/ybbrc

Cloning, expression, and characterization of recombinant nitric oxide synthase-like protein from *Bacillus anthracis* ☆

Shuchi Midha [a], Rajeev Mishra [b], Mohd. Azhar Aziz [a], Meenakshi Sharma [a], Ashish Mishra [a], Puneet Khandelwal [a], Rakesh Bhatnagar [a,*]

[a] *Center for Biotechnology, Jawaharlal Nehru University, New Delhi 110067, India*
[b] *Center for Computational Biology and Bioinformatics, Jawaharlal Nehru University, New Delhi 110067, India*

Received 5 August 2005
Available online 22 August 2005

Abstract

Nitric oxide synthase (NOS) is amongst a family of evolutionarily conserved enzymes, involved in a multi-turnover process that results in NO as a product. The significant role of NO in various pathological and physiological processes has created an interest in this enzyme from several perspectives. This study describes for the first time, cloning and expression of a NOS-like protein, baNOS, from *Bacillus anthracis*, a pathogenic bacterium responsible for causing anthrax. baNOS was expressed in *Escherichia coli* as a soluble and catalytically active enzyme. Homology models generated for baNOS indicated that the key structural features that are involved in the substrate and active site interaction have been highly conserved. Further, the behavior of baNOS in terms of heme–substrate interactions and heme-transitions was studied in detail. The optical perturbation spectra of the heme domain demonstrated that the ligands perturb the heme site in a ligand specific manner. baNOS forms a five-coordinate, high-spin complex with L-arginine analogs and a six-coordinate low-spin complex with inhibitor imidazole. Studies indicated that the binding of L-arginine, N^{ω}-hydroxy-L-arginine, and imidazole produces various spectroscopic species that closely correspond to the equivalent complexes of mammalian NOS. The values of spectral binding constants further corroborated these results. The overall conservation of the key structural features and the correlation of heme–substrate interactions in baNOS and mammalian NOS, thus, point towards an interesting phenomenon of convergent evolution. Importantly, the NO generated by NOS of mammalian macrophages plays a potent role in antimicrobicidal activity. Because of the existence of high structural and behavioral similarity between mammalian NOS and baNOS, we propose that NO produced by *B. anthracis* may also have a pivotal pathophysiological role in anthrax infection. Therefore, this first report of characterization of a NOS-like protein from a pathogenic bacterium opens up avenues for further studies in understanding the importance of this protein in pathogenicity.
© 2005 Elsevier Inc. All rights reserved.

Keywords: *Bacillus anthracis*; Nitric oxide synthase; Optical spectral perturbation; Heme–substrate interaction

Nitric oxide synthase (NOS) is a family of bimodal enzymes, comprising of an N-terminal oxygenase domain (NOSoxy) that binds protoporphyrin IX (heme), 6*R*-tetrahydrobiopterin (H_4B), and L-arginine (Arg); and a C-terminal reductase domain (NOSred) that binds FMN, FAD, and NADPH [1]. The two domains are linked together by a calmodulin (CaM) binding sequence [1]. CaM binding activates NO synthesis by triggering electron transfer from the flavins to heme [2]. Sequential transfer of electrons, thus, enables the heme to bind and activate oxygen in both steps of NO synthesis, resulting in NADPH- and

☆ *Abbreviations:* NOS, nitric oxide synthase; baNOS, *Bacillus anthracis* nitric oxide synthase; deiNOS, *Deinococcus radiodurans* nitric oxide synthase; bsNOS, *Bacillus subtilis* nitric oxide synthase; NOSoxy, nitric oxide synthase oxygenase domain; NOSred, nitric oxide synthase reductase domain; H_4B, (6*R*)-5,6,7,8-tetrahydrobiopterin; Ni–NTA, Ni^{2+}–nitrilotriacetic acid; DTT, dithiothreitol; EPPS, (*N*-[2-hydroxyethyl]piperazine-*N*′-[3-propanesulfonic acid]; HEPPS); BCIP, 5-bromo-4-chloro-3-indolyl phosphate disodium salt; NBT, nitro blue tetrazolium; PA, protective antigen; LF, lethal factor; EF, edema factor.

* Corresponding author. Fax: +91 11 26717040.
E-mail addresses: rakbhat01@yahoo.com, rakeshbhatnagar@mail.jnu.ac.in (R. Bhatnagar).

0006-291X/$ - see front matter © 2005 Elsevier Inc. All rights reserved.
doi:10.1016/j.bbrc.2005.08.083

O_2-dependent oxidation of L-Arg to NO and citrulline forming N^{ω}-hydroxy-L-arginine (NOHA) as an intermediate [3–5]. Thus, the overall reaction is similar to the mono-oxygenation reactions catalyzed by the cytochrome P450's [6,7].

Heretofore, mechanisms were deciphered that exclusively involve heme of NOS as the substrate-binding site. The heme pocket of NOS was envisaged to form the catalytic site where the stepwise oxidation of L-Arg to citrulline takes place [8,9]. It was found that heme of NOS was necessary for both the steps of monooxygenation reactions involved in the synthesis of NO [10,11]. The resting form of NOS (in the absence of L-Arg and H_4B) has ferric heme iron in a six-coordinated low-spin state. A switch from low-spin-hexacoordinate state to high-spin-pentacoordinate state was observed on H_4B and L-Arg binding [12,13]. This type of low-spin to high-spin transition was also observed in the cytochrome P450 group of enzymes [6].

Although much progress was made in unveiling the mechanism of action of eukaryotic nitric oxide synthases, corresponding reports in the prokaryotic counterparts were very few [14–16,36]. This was because of the fact that very few prokaryotic NOS-like proteins were cloned, completely sequenced, expressed, and purified. But with the successful completion of genome sequencing experiments, it was found that the NOS-like proteins existed in many eukaryotes and that these proteins have been conserved throughout evolution from prokaryota to eukaryota, suggesting their importance [17–21]. In spite of all this, the biological role of NO production by nitric oxide synthases in wide genera of intracellular pathogenic bacteria is still unknown.

The pathogenesis of *Bacillus anthracis* has been largely attributed to three non-toxic proteins—protective antigen (PA), lethal factor (LF, a Zn^{2+} metalloprotease), and edema factor (EF, a calmodulin- and calcium-dependent adenylate cyclase) that associate in binary combination to form two toxins, namely, lethal toxin (PA + LF), which causes cell death [22], and edema toxin (PA + EF), which is responsible for the edema seen in experimental animals [23,24]. The genes for protective antigen [25,26], lethal factor [27,28], and edema factor [29,30] were cloned, sequenced, expressed, and characterized, even before the *B. anthracis* genome was completely sequenced. Other than these three proteins, only a few other proteins have been studied in detail. Keeping in mind the important role of NO, we, therefore, describe in this communication the cloning, expression, and purification of a NOS-like protein from *B. anthracis*. NOS is a heme protein [31] and the heme iron has a proximal cysteine thiolate ligand [32–34]; therefore, we studied how the native substrate (L-Arg), intermediate (NOHA), and inhibitor (imidazole) interact with the heme site of baNOS.

Our results indicated that the heme iron of *B. anthracis* NOS-like protein is a predominantly high spin, pentacoordinate ferric species and that the binding of the substrates L-Arg and NOHA converts the remainder of the low-spin state species to high-spin state in titratable manner. Imidazole, a classic inhibitor of cytochrome P450, converted the protein to a low-spin state species.

Thus, our findings establish the exact nature of heme–substrate interactions and heme transitions taking place during L-arginine, NOHA, and imidazole binding to baNOS and clearly show that both mammalian NOS and baNOS show structural similarity and functional analogy in terms of heme–substrate interactions, and therefore, might be involved in performing a common primary function.

Experimental procedures

Materials. L-Arg, NOHA, H_4B, NADPH, FAD, FMN, EPPS, sodium nitrite, and anti-mouse IgG (whole molecule) $F(ab')_2$ fragment-alkaline phosphatase from sheep were obtained from Sigma. Sulfanilamide and naphthylethylenediamine were obtained from Himedia. The cloning vector pGEMT *Easy* was obtained from Promega, Cambridge, MA. Expression vector pET 29a was from Novagen. Restriction enzymes used for cloning were obtained from MBI, Fermentas. HIS-probe (H-3) used for Western blotting was obtained from Santa Cruz Biotechnology, Santacruz, CA. Ni–NTA agarose was obtained from Qiagen, Chatsworth, CA.

Cloning. Full-length structural gene for baNOS (1.1 kb) was amplified by PCR from *B. anthracis* (Sterne strain) genomic DNA. The primers utilized for amplification introduced *Bam*HI and *Hin*dIII sites at the 5′ and 3′ ends of the PCR product, respectively. The PCR product was cloned into pGEMT—*Easy* vector. This clone was restricted with *Bam*HI and *Hin*dIII, and the resulting fragment was purified by running it on 1% agarose gel. Expression vector pET 29a was also digested with *Bam*HI and *Hin*dIII enzymes, and the purified backbone was ligated with *Bam*HI and *Hin*dIII digested fragment obtained from pGEMT clone. The ligation product was transformed into *Escherichia coli* BL21 (*DE3*) competent cells. The clones that gave a fallout of 1.1 kb upon digestion with *Bam*HI and *Hin*dIII were selected (Fig. 1A). Sequencing of the construct was done to confirm that the full-length baNOS gene had been cloned between the *Bam*HI and *Hin*dIII sites of pET 29a.

Protein expression. Cell culture was performed at 37 °C in 1 L flasks containing LB broth with 50 μg/ml kanamycin. Protein expression was induced at an optical density of 0.5–0.7 at 600 nm by the addition of IPTG (1 mM). Cells were harvested 6–8 h post-induction by centrifugation and frozen at −80 °C until further use.

Protein purification. baNOS had His_6-tag attached to its C-terminus to aid purification. Protein was overexpressed in *E. coli* strain BL21 (*DE3*) by inducing the cells with IPTG (1 mM) and purified on Ni^{2+}–nitrilotriacetic acid resin. The frozen cells were thawed in approximately one-tenth of the total culture volume in buffer A (50 mM potassium phosphate buffer (pH 7.5), 300 mM NaCl, and lysozyme 100 mg/ml, pH 7.5). The cells were lysed by pulse sonication for 5 min and centrifuged at 14,000 rpm for 20 min. The supernatant was collected and re-centrifuged at 14,000 rpm for 60 min. The final supernatant was applied to Ni–NTA column pre-equilibriated with buffer B (buffer A + 20 mM imidazole). After loading the supernatant twice, the column was washed with three-column volumes of buffer B. The protein was eluted in buffer C (0.1 M Na_2HPO_4, 300 mM imidazole, pH 7.5). Eluted protein fractions were then pooled and dialyzed against buffer D (50 mM Tris–HCl, 10% glycerol, 0.1 M NaCl, 0.1 M EDTA, and 0.1 mM DTT, pH 7.5). The dialyzed protein was stored at −80 °C until further use. All manipulations in the protein purification process were performed at 4 °C.

Western blot. For Western blotting, both crude cell lysate and purified baNOS were electrophoresed on 12% polyacrylamide gel and transferred onto nitrocellulose membrane. The mixture was probed with 1:1000 dilution of HIS-probe (H-3) and then with sheep anti-mouse IgG

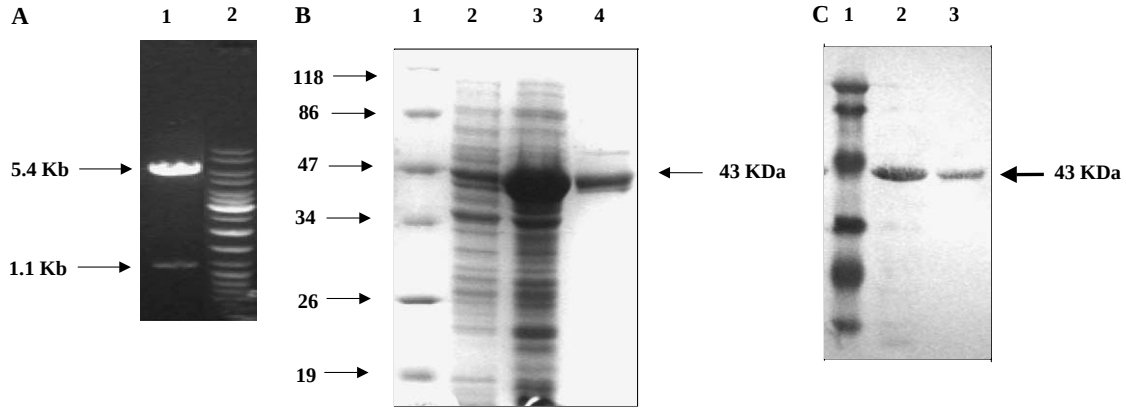

Fig. 1. (A) Restriction analysis of baNOS clone. Lane 1—baNOS digested with *Bam*HI and *Hin*dIII. The appearance of bands corresponding to 5.4 and 1.1 kb denotes pET29a plasmid backbone and NOS gene, respectively. (Lane 2)—1 kb Gene ladder. (B) SDS–PAGE analysis of total-cell lysate and purified protein. Lane 1—protein molecular weight marker. Lane 2—uninduced protein sample. Lane 3—induced protein sample. Lane 4—Ni^{2+}–NTA purified baNOS protein sample (corresponds to 43 kDa). (C) Western blot of total-cell lysate and purified protein. Lane 1—protein molecular weight marker. Lane 2—induced protein sample. Lane 3—Ni^{2+}–NTA purified baNOS protein sample (corresponds to 43 kDa).

alkaline-phosphatase-conjugated secondary antibody. The blot was developed with BCIP/NBT.

Protein determination. Protein concentration was determined by the Bradford dye binding micromethod [35] using bovine serum albumin as the standard.

Nitrite production. Nitrite production by *E. coli* lysates was measured by the Griess assay as described previously [36]. Briefly, N^{ω}-hydroxy-L-arginine (2 mM) and hydrogen peroxide (4 mM) were reacted with 20 μl of cell lysates and assayed for nitrite with Griess reagents after incubating for 15 min. Cell lysate with empty vector was kept as control.

Sequence alignment and comparative modeling. We used bsNOS (PDB code: 1M7V) and mammalian NOS (PDB code: 1OM4) as templates to generate the homology models of the baNOS. Multiple sequence alignments were carried out using ClustalW package [37]. In order to perform the secondary structure-based alignment of the template and target sequences, secondary structure of baNOS was predicted by Jpred [38] and 3D-PSSM [39] (www.bmm.icnet.uk/~3dpssm). These predictions were used to align the regions with the corresponding secondary structural elements of bsNOS and mammalian NOS, based on its three-dimensional structure. These alignments were used to build several homology models using MODELLER 6.v2 [40] (http://salilab.org), which generates energy minimized protein tertiary structures by satisfying spatial restraints imposed by the sequence alignment with the template structure and applying the terms of the CHARMM-22 force-field. The best model was selected according to the objective function suggested by Modeller [40]. We used the program PROCHECK [41] to evaluate the predicted model based on the stereochemical and geometric considerations.

Superposition of Cα traces and backbones of the models onto the template crystal structure was compared using DeepView/Swiss-Pdb-Viewer 3.7 (http://www.expasy.org/spdbv/). The figures were created using the software CHIMERA (http://www.cgl.ucsf.edu/chimera).

Arginine and H_4B binding. Arginine and H_4B binding affinity was studied at 25 °C spectrophotometrically according to methods described previously [16]. Briefly, the enzyme (2 μg) was taken in a buffer, which contained 40 mM EPPS, 10% glycerol, 1 mM DTT, and 20 μM H_4B. Spectra were recorded after incubating baNOS for 15 min at 25 °C under the conditions indicated.

Optical perturbation difference spectroscopy. Substrate perturbation difference spectroscopy measurements were conducted in the absence of added tetrahydrobiopterin. Optical spectra were recorded using Jasco Model V-530 UV/visible spectrophotometer, with Peltier temperature control accessory, and in 1.0 ml quartz cuvettes. Titration experiments were performed at 10 or 15 °C as described previously [42].

Determination of K_s for L-Arg, NOHA, and imidazole. The spectral binding constants, K_s, were determined from the *x*-intercept of a double-reciprocal plot of the difference in the respective peak to trough absorbances versus the perturbant concentration.

Results and discussion

Cloning, expression, and purification

We cloned the 1.1 kb NOS gene of *B. anthracis* (Sterne strain) by amplifying it by PCR from genomic DNA (Fig. 1A). This fragment coded for a 356 amino acid nitric oxide synthase-like protein and SDS–PAGE profile showed that baNOS migrates at 43 kDa, which correlates well with its molecular weight (Fig. 1B). The specificity of the protein was further confirmed by Western blot by probing it with HIS-probe (H3) as the expressed protein had His_6-tag attached to its C-terminal (Fig. 1C). Further, the recombinant protein was purified using metal–chelate affinity chromatography (Ni^{2+}–NTA column). The 6× His-tag at the C-terminus facilitated strong binding of the protein to the Ni–NTA matrix. Most of the cytosolic proteins were washed away from the column with 20 mM imidazole. SDS–PAGE analysis revealed that the metal affinity chromatography purified baNOS migrated as a single band and had purity of more than 95%. It was possible to achieve a yield of ~9 mg of purified protein from 1 L of culture broth. Cell lysates expressing baNOS generated nitrite at a concentration significantly above that of the empty vector control (pET 29a). The selective mammalian NOS inhibitor NMA (N^{G}-methyl arginine) inhibited nitrite formation by lysates expressing baNOS at a final concentration of 1 mM (Fig. 2).

Primary sequence analysis

The sequence analysis of baNOS, rat brain NOS, and bsNOS indicates that baNOS has 52% identity with bsNOS and 45.2% identity with rat brain NOS (Fig. 3). It also indicates sequence homology at other structural

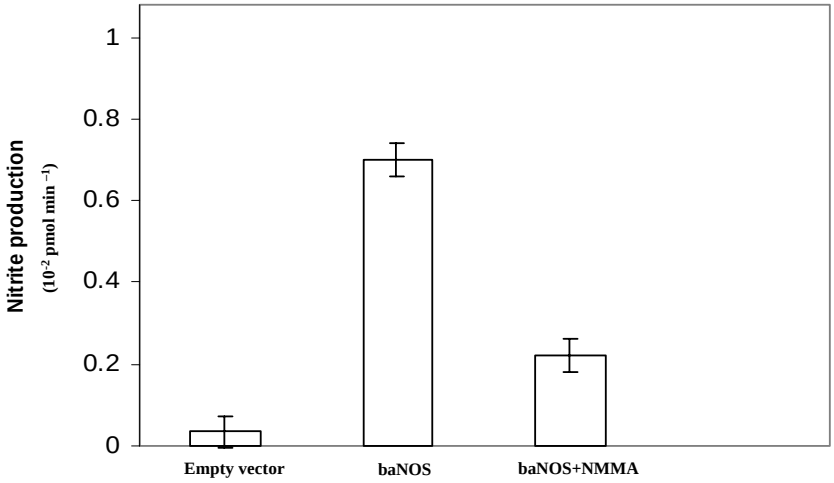

Fig. 2. Nitrite formation from N^{ω}-hydroxy-L-arginine by recombinant baNOS. (Bars indicate standard error; $n = 5$.)

Fig. 3. Comparative analysis of primary protein sequence of baNOS, bsNOS, and mammalian NOS. Secondary structure-based sequence alignment of bsNOS (top), rat brain NOS (middle), and baNOS (bottom) with mapped residue function and contributions to the dimer interface as determined from iNOSoxy structures [47]. NOS sequences are color-coded to highlight zinc ligands Cys30 and Cys36, and proximal heme ligand Cys119 (yellow background), Arg-binding residue (blue block), and H_4B-binding residues (red block). Black arrows show β sheets, thick boxes show α helices. Key sequence stretches involved in forming the dimer interface and cofactor-binding sites are boxed in magenta and denoted as N-terminal hook, switch region (zinc loop), N-terminal pterin binding, helical T, and helical lariat. (For interpretation of the references to colour in this figure legend, the reader is referred to the web version of this paper.)

residues, which contact heme, H_4B, and L-Arg. Also, the elements that make up the catalytic core in mammalian NOS are well conserved in baNOS. Like the previously identified deiNOS and bsNOS, baNOS also lacks an extended N-terminal sequence found in mammalian enzymes. This N-terminal sequence in mammalian enzymes codes for a N-terminal hook and metal binding site, and contains residues that participate in forming the dimer interface and binding the dihydroxypropyl side chain of H_4B [43].

Thus, the finding of sequence similarity at the catalytic core and the conservation of key elements between baNOS, bsNOS, and mammalian NOS supports the contention that these proteins have evolved through an interesting phenomenon of convergent evolution [44].

Homology modeling studies

Homology modeling studies suggest that the substrates, L-Arg and NOHA, bind to the active site in

baNOS in a manner similar to that in bsNOS and mammalian NOS (Figs. 4A and B). But the substrate access channel is very much wide in baNOS, as compared to that in mammalian NOS due to the lack of N-terminal hook. In spite of this difference, the residues that interact with L-Arg and NOHA, and their overall positioning with respect to the active center are similar. This results in the binding of L-Arg and NOHA between the heme and side chain of Pro214 of baNOS. Two other residues namely, Glu235 and Trp234, interact with the bridging guanidium nitrogen and terminal nitrogen atom of L-Arg, which results in directing the L-Arg guanidium nitrogen to the open coordination site of heme iron for oxygen activation during NO synthesis. Other analogous interactions include those with Tyr237, Asn246, and Gln129 that interact with the carboxyl group of L-Arg and NOHA. Also, the bacterial NOS proteins contain conserved Ile216 corresponding to a Val residue of mammalian NOS. This residue does not seem to block the access of substrate channel.

The key structural residues that interact with L-Arg and NOHA are conserved, except for a Gly235 that forms a hydrogen bond with the hydroxyl group of NOHA. Therefore, the conservation of the key residues of the active site indicates a high level of similarity in the substrate and active site interactions in baNOS and mammalian NOS.

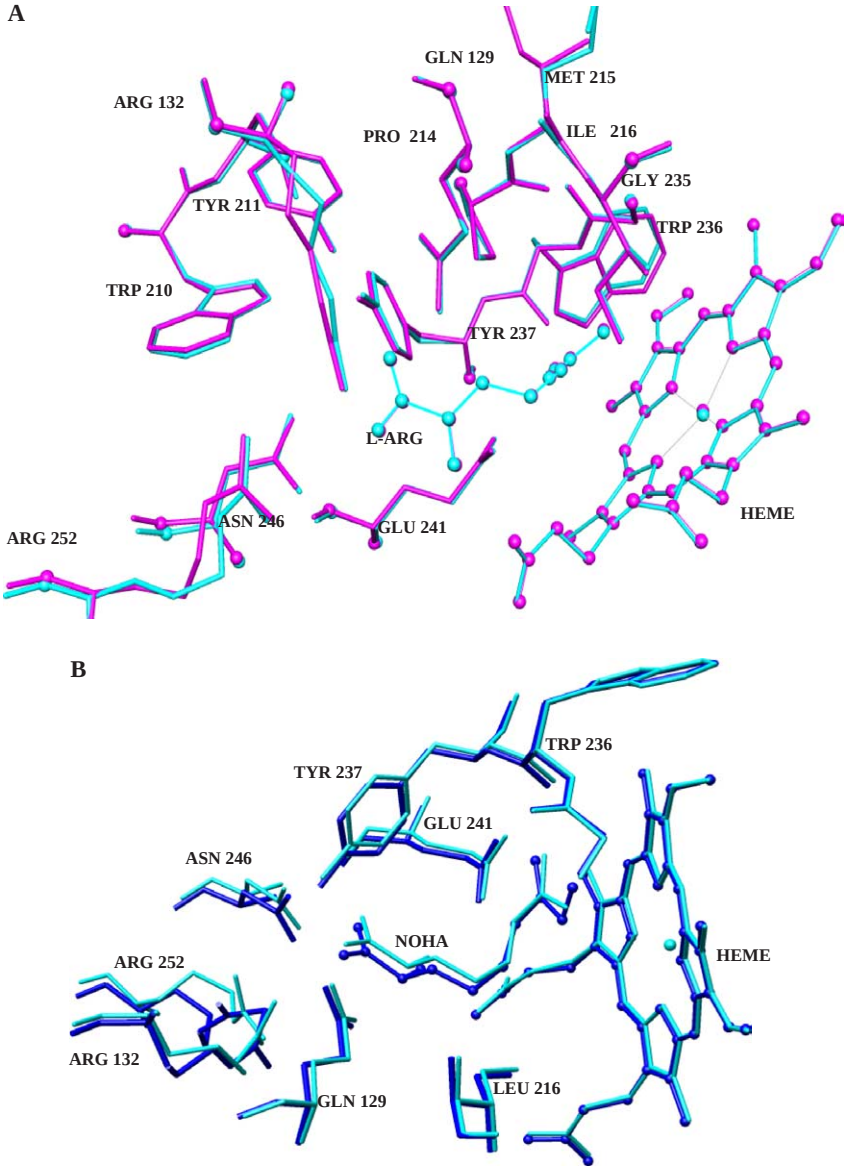

Fig. 4. (A) Stereoview of baNOS-binding site for L-arginine. Superposition of residues in the active sites of bsNOS (magenta) and baNOS (cyan). All the residues that contribute to L-arginine binding are highly conserved, except for a conserved change in the heme pocket of bacterial NOS proteins, which contain Ile216 instead of a Val residue of mammalian NOS. This residue does not seem to block the access of substrate channel. But might affect the rate of NO dissociation. (B) Stereoview of baNOS binding site for N^{ω}-hydroxy-L-arginine. Superposition of residues in the active sites of mammalian NOS (blue) and baNOS (cyan). All the residues contributing to N^{ω}-hydroxy-L-arginine binding are highly conserved. (For interpretation of the references to colour in this figure legend, the reader is referred to the web version of this paper.)

Absolute spectral characteristics

The optical absorption spectrum of the purified resting enzyme baNOS (without added L-Arg) is an indicative of a predominantly high-spin state of heme iron, as judged by the broad peak at λ_{max} 390 nm (Fig. 5A). The predominantly high-spin enzyme preparation (~80%) has a fraction of heme population in the low-spin state characterized by a shoulder ~410 nm. This is in analogy with the ferric cytochrome P450 enzymes and other heme proteins with *b-type* heme prosthetic group, whereby, they display Soret peaks at ~390 nm and ~410 nm corresponding to the presence of both high-spin-state heme iron and low-spin-state heme iron, respectively [42].

Spectral changes obtained upon DTT, L-Arg, and H_4B bindings are shown in Fig. 6. Ferric baNOS showed characteristic absorbance maxima at 410 and 390 nm, indicating its heme-bound DTT to form a bisthiolate species identical to mammalian NOS [45]. Addition of H_4B is followed by the disappearance of the shoulder at 410 nm and produces a broad Soret band centered at 400 nm, indicating a mixture of high- and low-spin-state heme iron. This structural change is probably facilitated by the formation of hydrogen bonds between H_4B and one of the heme propionate groups [33,46]. Addition of L-Arg to H_4B bound baNOS converted the remaining low-spin heme iron into a high-spin form. The absorbance excursion $(A_{\text{after L-Arg addition}} - A_{\text{after } H_4B \text{ addition}})$ of 0.015 AU suggests that the increase was largely attributable to L-Arg alone, as shown in Fig. 5. This finding is consistent with the previous observations with both iNOS [47] and nNOS [48]. Therefore, this provides convincing evidence that pterin factor binding in baNOS occurs at the heme site in a manner equivalent to that in eukaryotic counterparts and further point the co-localization of L-Arg and pterin binding site to be within the amino terminal half of baNOS molecule.

Optical perturbation difference spectroscopy

Nitric oxide synthases contain a *b-type* heme, axially ligated to the thiolate side chain of an implicitly conserved cysteine residue [32–34,49,50], which reacts with CO in the presence of NADPH to give an absorbance peak at 444–448 nm. This seminal finding became the mechanistic fulcrum in applying much of our understanding of cytochrome P450 biochemistry to NOS, thus, further creating interest in understanding the active site, i.e., heme-binding site in nitric oxide synthases. In this context, difference spectrophotometry defined the active site structure of baNOS in close comparison with that of cytochrome P450's and allowed the close monitoring of subtle changes which were happening as a result of substrate and inhibitor binding at the heme site in baNOS. Thus, this technique was used successfully in probing the heme site of an enzyme from prokaryotic origin.

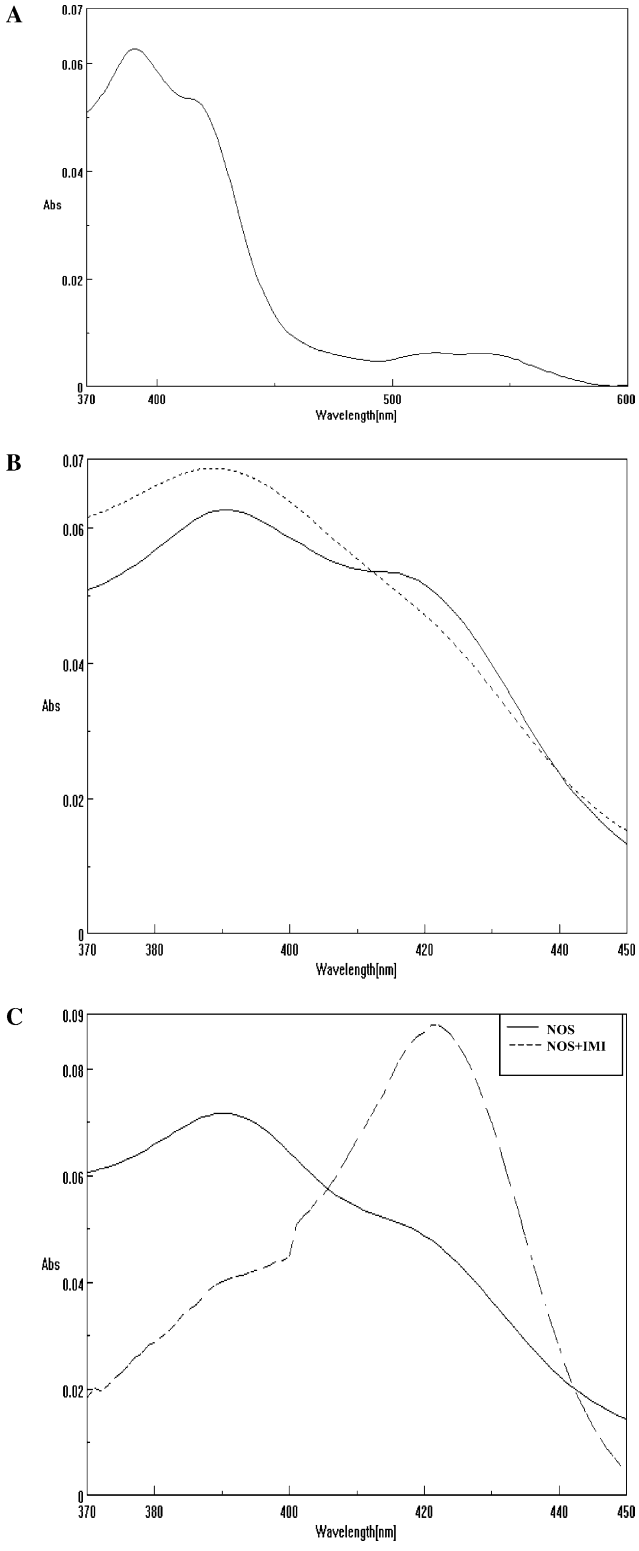

Fig. 5. (A) Absolute spectrum of baNOS. Spectrum of baNOS (1.9 μM) in 50 mM Tris–HCl, pH 7.5, and 10% glycerol with a final volume change less than 1%. (B) Absolute spectrum of baNOS after the addition of L-Arg. Spectrum of baNOS (1.9 μM) after the addition of L-arginine (1.8 μM) in 50 mM Tris–HCl, pH 7.5, and 10% glycerol with a final volume change less than 1%. (C) Absolute spectrum of baNOS after the addition of imidazole. Spectrum of baNOS (1.9 μM) after the addition of imidazole (1 mM) in 50 mM Tris–HCl, pH 7.5, and 10% glycerol with a final volume change less than 1%.

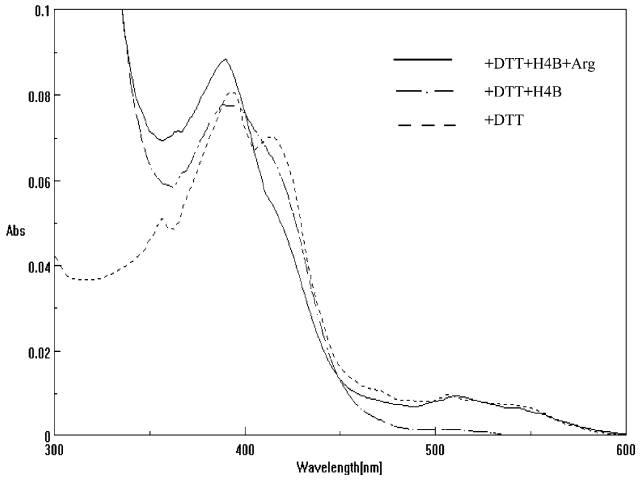

Fig. 6. Spectrum of DTT bound baNOS and displacement of DTT upon H_4B and L-Arg binding. Spectra were recorded after incubating baNOS for 15 min at 25 °C under the conditions indicated.

Type I perturbation difference spectra

The bound heme group provides a spectral probe to monitor how the heme environment changes during the binding of substrates. The changes in the heme pocket architecture were monitored by spectral perturbation effects. The baNOS heme–substrate interactions were found to be H_4B independent, as the spectral perturbations were observed in the absence of added H_4B. Fig. 4B shows the absolute spectrum of baNOS after L-Arg addition, which displays a peak at ~390 nm, suggesting the formation of high-spin iron (III) form as a result of the replacement of the endogenous ligand responsible for the high-spin state with L-Arg or the slow dissociation of the ligand from the heme-binding site upon dilution of the enzyme. By analogy with the substrate binding interactions with cytochrome P450's, e.g., hexobarbital with microsomal cytochromes P450 [51], the substrate perturbation difference spectra obtained for the native substrate L-Arg with baNOS exhibited "type I" substrate perturbation difference spectra characterized by the appearance of a peak at ~390 nm and a trough at ~410 nm. Upon sequential addition of L-Arg to baNOS, there was a concentration dependent spectral shift which indicated that L-Arg could completely convert hexa-coordinate low-spin-state heme iron into penta-coordinate high-spin-state heme iron in an otherwise mixed population of enzyme preparation (Fig. 7A). Similarly, Fig. 8A shows the spectral perturbation obtained upon titration with NOHA, which is quite similar to that obtained with L-Arg. The minor differences in the perturbations might be due to the presence of the hydroxyl group in NOHA. But, indeed, it is expected that the type I ligands, L-Arg and NOHA, will bind at the same site in an extended conformation, fitting into a narrow part of the active site cavity coplanar to heme. The spectral binding constant (K_s), the concentration of the perturbant resulting in half the maximal theoretical spectral change, was obtained from the double reciprocal plot of the absorbance differences versus substrate concentration. The K_s value for L-Arg was found to be 1.17 μM (Fig. 7B) and for NOHA it was 1.33 μM (Fig. 8B), which indicated high substrate binding affinity. These values were in agreement with the previously reported kinetic constant for L-Arg binding to mammalian NOS, $K_m = \sim 2$ μM [42].

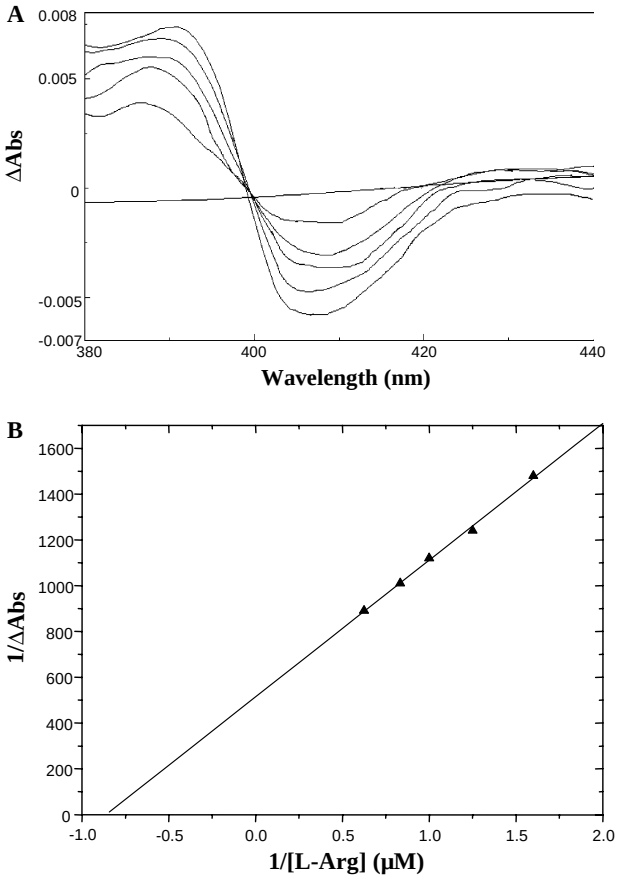

Fig. 7. (A) L-Arginine perturbation difference spectra. The titrations were performed in 0.5 ml aliquots of 2.2 μM baNOS. Both the sample and reference cuvettes were maintained at 10 °C in spectrophotometer. The baseline was adjusted to zero absorbance. Additions of L-arginine in 50 mM Tris–HCl, pH 7.5, and 10% glycerol were made to the sample cuvette. The spectrum was recorded from 350 to 450 nm following each addition. The final concentrations of L-arginine were (a) baseline, (b) 0.60 μM, (c) 0.80 μM, (d) 1.0 μM, (e) 1.2 μM, and (f) 1.6 μM, respectively. The total volume change was less than 2%. (B) Determination of spectral binding constant (K_s) for L-arginine. Difference spectra of baNOS L-arginine titrations were performed using 2.2 μM baNOS and L-arginine concentrations ranging from 0.60 to 1.6 μM. The absorbance differences ($A_{380} - A_{420}$) versus [L-arginine] are plotted as a double-reciprocal plot. The value of K_s was derived from the x-intercept.

Thus, it concludes that the native substrate L-Arg binds with high affinity to the heme moiety of baNOS in a type I manner and that the binding of N^{ω}-hydroxy-L-arginine (NOHA) to baNOS shows a similar orientation pattern in the active site as L-arginine. This fact was also confirmed by the homology modeling studies, which indicated that

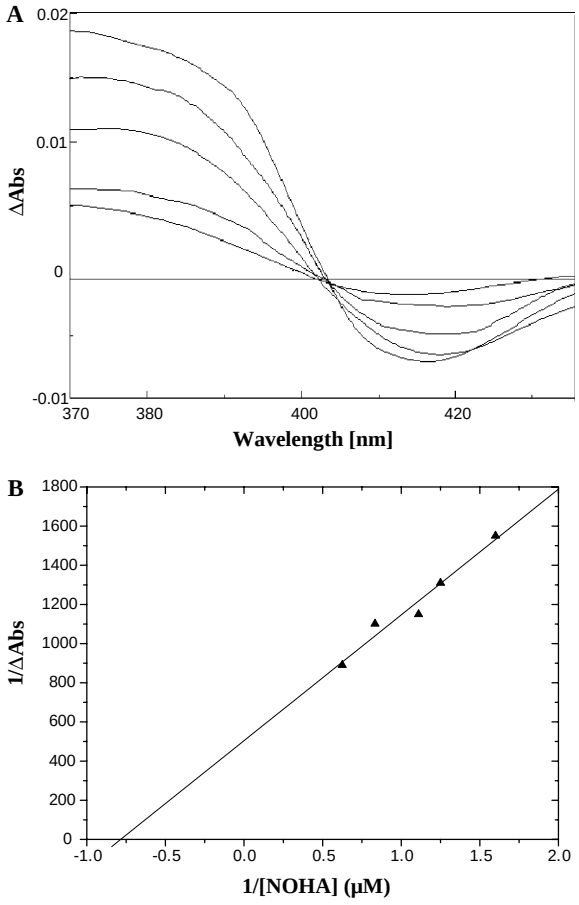

Fig. 8. (A) N^{ω}-Hydroxy-L-arginine perturbation difference spectra. Titration of baNOS (3.0 μM) with N^{ω}-hydroxy-L-arginine was performed at 15 °C, as described in Fig. 6A. The final concentrations of N^{ω}-hydroxy-L-arginine were (a) baseline, (b) 0.60 μM, (c) 0.80 μM, (d) 1.0 μM, (e) 1.2 μM, and (f) 1.6 μM, respectively. The total volume change was less than 2%. (B) Determination of spectral binding constant (K_s) for N^{ω}-hydroxy-L-arginine. Difference spectra of baNOS N^{ω}-hydroxy-L-arginine titrations were performed using 3.0 μM baNOS and N^{ω}-hydroxy-L-arginine concentrations ranging from 0.60 to 1.6 μM. The absorbance differences ($A_{380} - A_{420}$) versus [N^{ω}-hydroxy-L-arginine] are plotted as a double-reciprocal plot. The value of K_s was derived from the x-intercept.

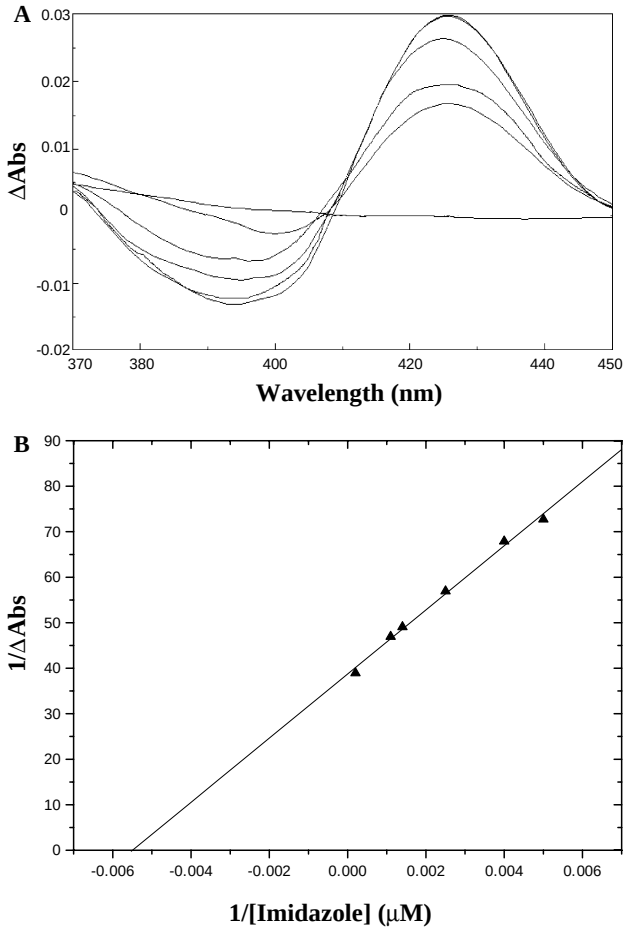

Fig. 9. (A) Imidazole perturbation difference spectra. Titration of baNOS (2.2 μM) with imidazole was performed at 15 °C, as described in this figure. The final concentrations of imidazole were (a) baseline, (b) 200 μM, (c) 250 μM, (d) 400 μM, (e) 700 μM, and (f) 900 μM, (g) 1 mM, respectively. The total volume change was less than 2%. (B) Determination of spectral binding constant (K_s) for imidazole. Difference spectra of baNOS imidazole titrations were performed using 2.2 μM baNOS and imidazole concentrations ranging from 200 μM to 1 mM. The absorbance differences ($A_{430} - A_{390}$) versus [imidazole] are plotted as a double-reciprocal plot. The value of K_s was derived from the x-intercept.

L-Arg and NOHA bind with their guanidium, and hydroxyguanidium groups stacked between heme prosthetic group and Pro214. These findings were found to be consistent with mammalian NOS.

Type II perturbation difference spectra

Imidazole has been observed to bind diverse cytochrome P450 isoforms [52–54]. The addition of imidazole (1 mM) to baNOS resulted in the conversion of the total enzyme present to a low-spin state characterized by a peak at $\lambda_{max} \sim 430$ nm (Fig. 5C). The 430 nm species is a six-coordinate low-spin heme with imidazole as the sixth axial ligand. Titration of baNOS with imidazole resulted in difference perturbation spectra shown in Fig. 9A. It was characterized by gradual conversion of the predominantly high-spin state heme iron to low-spin state with a K_s value for imidazole binding to be around 181 μM (Fig. 9B). Further, upon titration of imidazole–baNOS complex with L-Arg, the binding of imidazole to the ferric iron was disrupted as evident from the spectral shift (Fig. 10A). The binding of L-Arg to the baNOS–imidazole complex induced a blueshift from 430 to 390 nm, indicating the restoration of the high-spin state enzyme–substrate complex, which was independent of the presence of imidazole. The fact was further confirmed by the spectral binding constant value for L-Arg in the presence of imidazole, which was found to be 2.5 μM (Fig. 10B), suggesting that L-Arg is capable of displacing the bound inhibitor. This suggests a link between the binding site of imidazole and L-Arg. The formation of a ternary complex between NOS, imidazole, and L-Arg is, therefore, speculated, whereby, imidazole binds the heme iron at the sixth axial ligand site characterized by the appearance of type II difference spectrum.

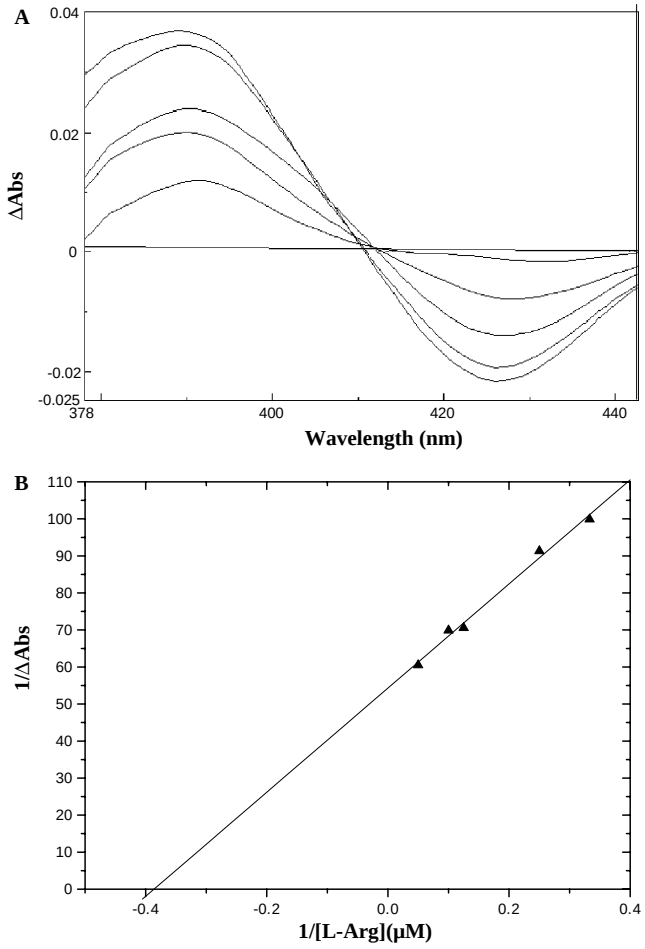

Fig. 10. (A) Titration of imidazole-induced low-spin-state baNOS with L-arginine. Imidazole was added to a final concentration of 1 mM to both the sample and reference cuvettes, and the baseline was recorded. Additions of L-arginine were made to the sample cuvette with resulting final concentrations of (a) baseline, (b) 3.0 μM, (c) 4.0 μM, (d) 8.0 μM, (e) 10 μM, and (f) 20 μM, respectively. (B) Determination of spectral binding constant (K_s) for L-arginine in the presence of imidazole. Difference spectra obtained from the titrations of imidazole bound baNOS with L-arginine were performed using 2.2 μM baNOS bound with imidazole (1 mM) and L-arginine concentrations ranging from 3.0 to 20 μM. The absorbance differences ($A_{390} - A_{430}$) versus [L-arginine] are plotted as a double-reciprocal plot. The value of K_s was derived from the x-intercept.

Conclusively, these spectra of baNOS complexed with these ligands conglomerated with the previous findings with mammalian NOS.

The existence of fundamental structural and functional similarity between the two enzyme families, i.e., baNOS and mammalian NOS, therefore, points towards the occurrence of convergent evolution. Both display absorption peaks in the Soret and the visible region at nearly the same positions. Also for these enzyme families, the resting state (or substrate free) heme iron is axially ligated by the thiolate side chain of an implicitly conserved cysteine residue and a labile water molecule. In the low-spin state, it is in the iron(II) form. Substrate binding causes a spin state shift from low- to high-spin iron(III) heme. In some cases, there is an associated increase in the heme reduction potential [55]. This increase in the heme reduction potential is thought to render heme reduction thermodynamically favorable once the substrate is bound, preventing uncoupled consumption of NADPH in the absence of substrate [55,56].

Thus, owing to the parallels that can be drawn from mammalian NOS to baNOS, it can be proposed that the two gene families have evolved through convergent evolution. Further, gene fusion events in a series led to evolution of structurally more complex and dimeric mammalian nitric oxide synthases, which are characterized by the occurrence of both, a flavin-containing reductase domain exhibiting structural and functional similarities with cytochrome P450, and a monooxygenase domain from the prokaryotic counterpart, all arranged within one linear polypeptide chain.

Despite all the valuable information available regarding this complex single-enzyme catalyzed reaction, the biological role of NO production by the NOS-like proteins in prokaryotes is currently unknown. Moreover, it becomes especially pertinent to decipher its role in an intracellular pathogenic bacterium like *B. anthracis*, causative agent for anthrax, which also has the potential to be used as a biological warfare agent. Therefore, it would be an interesting line of study to investigate its importance in the intracellular survival or viability of this organism. Also, this bacterium secretes three non-toxic proteins-protective antigen (PA), lethal factor (LF, a Zn^{2+} metalloprotease), and edema factor (EF, a calmodulin- and calcium-dependent adenylate cyclase) that associate in binary combination to form two toxins, namely, lethal toxin (PA + LF), which causes cell death and edema toxin (PA + EF), which is responsible for the edema seen in the disease [57–59]. There have been reports on the functional interrelationship between NO, cAMP levels, and platelet function inhibition [60–62]. Keeping this in mind and the fact that edema toxin causes edema by elevating cAMP levels to impair phagocyte function the context becomes even more important, suggesting a role for NO in edema toxin activity. Thus, these preliminary heme–substrate interaction studies in a NOS-like protein from *B. anthracis* will open up avenues to the understanding of NO biology in intracellular pathogenic microorganisms that may have far-reaching implications.

Acknowledgments

We thank Dr. Subrata Adak, Division of Infectious Diseases, Indian Institute of Chemical Biology, Kolkata, West Bengal, for encouraging the *B. anthracis* NOS project in our laboratory. We also thank Prof. Rajiv Bhat for his intellectual inputs during the course of discussion. Shuchi Midha is a recepient of Junior Research Fellowship Award by Council of Scientific and Industrial Research, Government of India, New Delhi, India.

References

[1] O.W. Griffith, D.J. Stuehr, Nitric oxide synthases properties and catalytic mechanism, Annu. Rev. Physiol. 57 (1995) 707–736.

[2] H.M. Abu-Soud, D.J. Stuehr, Nitric oxide synthases reveal a role for calmodulin in controlling electron transfer, Proc. Natl. Acad. Sci. USA 90 (1993) 10769–10772.

[3] H.M. Abu-Soud, R. Gachhui, F.M. Raushel, D.J. Stuehr, The ferrous-dioxy complex of neuronal nitric oxide synthase: divergent effects of L-arginine and tetrahydrobiopterin on its stability, J. Biol. Chem. 272 (1997) 17349–17353.

[4] N. Bec, A.C.F. Gorren, C. Voelkar, B. Mayer, R. Lange, Reaction of neuronal nitric-oxide synthase with oxygen at low temperature, J. Biol. Chem. 273 (1998) 13502–13508.

[5] D.J. Stuehr, J. Santolini, Z. Wang, C. Wei, S. Adak, Update on mechanism and catalytic regulation in the NO synthases, J. Biol. Chem. 279 (2004) 36167–36170.

[6] M.A. Marletta, A.K. Hurshman, K.M. Rusche, Catalysis by nitric oxide synthase, Curr. Opin. Chem. Biol. 2 (1998) 656–663.

[7] B. Hemmens, B. Mayer, in: M.A. Titheradge (Ed.), Enzymology of Nitric Oxide Synthases, Methods in Molecular Biology, vol. 100, Humana Press, Totowa, NJ, 1997, pp. 1–32.

[8] D.J. Stuehr, N.S. Kwon, C.F. Nathan, O.W. Griffith, P.L. Feldman, J. Wiseman, *N*-omega-hydroxy-L-arginine is an intermediate in the biosynthesis of nitric oxide from L-arginine, J. Biol. Chem. 266 (1991) 6259–6263.

[9] P. Klatt, K. Schmidt, G. Uray, B. Mayer, Multiple catalytic functions of brain nitric oxide synthase. Biochemical characterization, cofactor-requirement, and the role of *N* omega-hydroxy-L-arginine as an intermediate, J. Biol. Chem. 268 (1993) 14781–14787.

[10] D.J. Stuehr, M. Ikeda-Saito, Spectral characterization of brain and macrophage nitric oxide synthases. Cytochrome P-450-like hemeproteins that contain a flavin semiquinone radical, J. Biol. Chem. 267 (1992) 20547–20550.

[11] R.A. Pufahl, M.A. Marletta, Oxidation of N^{G}-hydroxy-L-arginine by nitric oxide synthase: evidence for the involvement of the heme in catalysis, Biochem. Biophy. Res. Commun. 193 (1993) 963–970.

[12] J. Wang, D.J. Stuehr, M. Ikeda-Saito, D.L. Rousseau, Heme coordination and structure of the catalytic site in nitric oxide synthase, J. Biol. Chem. 268 (1993) 22255–22258.

[13] L.J. Roman, E.A. Sheta, P. Marta Sek, S.S. Gross, W.C. Sessa, B.S. Masters, High-level expression of functional rat neuronal nitric oxide synthase in *Escherichia coli*, Proc. Natl. Acad. Sci. USA 92 (1995) 8428–8432.

[14] W.S. Choi, M.S. Chang, J.W. Han, S.Y. Hong, H.W. Lee, Identification of nitric oxide synthase in *Staphylococcus aureus*, Biochem. Biophy. Res. Commun. 237 (1997) 554–558.

[15] S. Adak, A.M. Bilwes, K. Panda, D. Hosfield, K.S. Aulak, J.F. McDonald, J.A. Tainer, E.D. Getzoff, B.R. Crane, D.J. Stuehr, Cloning, expression, and characterization of a nitric oxide synthase protein from *Deinococcus radiodurans*, Proc. Natl. Acad. Sci. USA 99 (2002) 107–112.

[16] S. Adak, K.S. Aulak, D.J. Stuehr, Direct evidence for nitric oxide production by a nitric-oxide synthase-like protein from *Bacillus subtilis*, J. Biol. Chem. 277 (2002) 16167–16171.

[17] U. Muller, The nitric oxide system in insects, Prog. Neurobiol. 51 (1997) 363–381.

[18] D.F. Klesig, J. Durner, R. Noad, D.A. Navarre, D. Wendehenne, D. Kumar, J.M. Zhou, J. Shah, S. Zhang, P. Kachroo, et al., Nitric oxide and salicylic acid signaling in plant defense, Proc. Natl. Acad. Sci. USA 97 (2000) 8849–8855.

[19] G. Golderer, E.R. Werner, S. Leitner, P. Grobner, G. Werner-Felmayer, Nitric oxide synthase is induced in sporulation of *Physarum polycephalum*, Genes Dev. 15 (2001) 1209–1299.

[20] H. Ninnemann, J. Maier, Indications for the occurrence of nitric oxide synthases in fungi and plants and the involvement in photoconidiation of *Neurospora crassa*, Photochem. Photobiol. 64 (1996) 393–398.

[21] M.W. Radomski, J.F. Martin, S. Moncada, Synthesis of nitric-oxide by the hemocytes of the american horseshoe-crab (limulus-polyphemus), Philos. Trans. R. Soc. London B 334 (1991) 129–133.

[22] A.M. Friedlander, Macrophages are sensitive to anthrax lethal toxin through an acid-dependent process, J. Biol. Chem. 261 (1986) 7123–7126.

[23] S.H. Leppla, Anthrax toxin edema factor: a bacterial adenylate cyclase that increases cyclic AMP concentrations of eukaryotic cells, Proc. Natl. Acad. Sci. USA 79 (1982) 3162–3166.

[24] P. Kumar, N. Ahuja, R. Bhatnagar, Purification of anthrax edema factor from *Escherichia coli* and identification of residues required for binding to protective antigen, Infect. Immun. 69 (2001) 6532–6536.

[25] M.H. Vodkin, S.H. Leppla, Cloning of the protective antigen gene of *Bacillus anthracis*, Cell 34 (1983) 693–697.

[26] P. Gupta, S.M. Waheed, R. Bhatnagar, Expression and purification of the recombinant protective antigen of *Bacillus anthracis*, Prot. Exp. Pur. 16 (1999) 369–376.

[27] T. Bragg, D.L. Robertson, Nucleotide sequence and analysis of the *Bacillus anthracis* lethal factor gene (lef), Gene 81 (1989) 45–54.

[28] P. Gupta, S. Khetarpal, A.P. Chopra, Y. Singh, R. Bhatnagar, Expression and purification of the recombinant lethal factor of *Bacillus anthracis*, Infect. Immun. 66 (1998) 862–865.

[29] D.L. Robertson, M.T. Tippetts, S.H. Leppla, Nucleotide sequence of the *Bacillus anthracis* edema factor gene (cya): a calmodulin-dependent adenylate cyclase, Gene 73 (1988) 363–371.

[30] P. Kumar, N. Ahuja, R. Bhatnagar, Anthrax edema toxin requires influx of calcium for inducing cAMP toxicity in target cells, Infect. Immun. 70 (2002) 4997–5007.

[31] K.A. White, M.A. Marletta, Nitric oxide synthase is a cytochrome P-450 type hemoprotein, Biochemistry 31 (1992) 6627–6631.

[32] T.O. Fischmann, A. Hruza, X.D. Niu, J.D. Fossetta, C.A. Lunn, E. Dolphin, A.J. Prongay, P. Reichert, D.J. Lundell, S.K. Narula, P.C. Weber, Structural characterization of nitric oxide synthase isoforms reveals striking active-site conservation, Nat. Struct. Biol. 6 (1999) 233–242.

[33] D.S. Bredt, S.H. Synder, Nitric oxide: a physiologic messenger molecule, Annu. Rev. Biochem. 63 (1994) 175–195.

[34] C.S. Raman, H. Li, P. Martasek, V. Kral, B.S. Masters, T.L. Poulos, Crystal structure of constitutive endotelial nitric oxide synthase: a paradigm for pterin function involving a novel metal center, Cell 95 (1998) 939–950.

[35] M.M. Bradford, Rapid and sensitive method for quantitation of microgram quantities of protein utilizing the principle of protein-dye, Anal. Biochem. 72 (1967) 248–254.

[36] J.A. Kers, M.J. Wach, S.B. Krasnoff, J. Widom, K.D. Cameron, R.A. Bukhalid, D.M. Gibson, B.R. Crane, R. Loria, Nitration of a peptide phytotoxin by bacterial nitric oxide synthase, Nature 429 (2004) 79–82.

[37] J.D. Thompson, D.G. Higgins, T.J. Gibson, CLUSTAL W: improving the sensitivity of progressive multiple sequence alignment through sequence weighting, position-specific gap penalties and weight matrix choice, Nucleic Acids Res. 22 (1994) 4673–4680.

[38] J.A. Cuff, M.E. Clamp, A.S. Siddiqui, M. Finlay, G.J. Barton, Jpred: a consensus secondary structure prediction server, Bioinformatics 14 (1998) 892–893.

[39] L.A. Kelley, R.M. MacCallum, M.J. Sternberg, Enhanced genome annotation using structural profiles in the program 3D-PSSM, J. Mol. Biol. 299 (2000) 499–520.

[40] A. Fiser, A. Sali, Modeller: generation and refinement of homology-based protein structure models, Methods Enzymol. 374 (2003) 461–491.

[41] R.A. Laskowski, M.W. MacArthur, D.S. Moss, J.M. Hornton, PROCHECK: a program to check the stereochemical quality of protein structures, J. Appl. Cryst. 26 (1993) 283–291.

[42] K. McMillan, B.S.S. Masters, Optical difference spectrophotometry as a probe of rat brain nitric oxide synthase heme–substrate interaction, Biochemistry 38 (1993) 9875–9880.

[43] B.R. Crane, R.J. Rosenfeld, A.S. Arvai, D.K. Ghosh, S. Ghosh, J.A. Tainer, D.J. Stuehr, E.D. Getzoff, N-terminal domain swapping and

metal ion binding in nitric oxide synthase dimerization, EMBO J. 18 (1999) 6271–6281.
[44] K. McMillan, B.S.S Masters, Prokaryotic expression of the heme- and flavin-binding domains of rat neuronal nitric oxide synthase as distinct polypeptides: identification of the heme-binding proximal thiolate ligand as cysteine-415, Biochemistry 34 (1995) 3686–3693.
[45] S. Adak, Q. Wang, D.J. Stuehr, Arginine conversion to nitroxide by tetrahydrobiopterin-free neuronal nitric-oxide synthase. Implications for mechanism, J. Biol. Chem. 275 (2000) 33554–33561.
[46] C. Jung, D.J. Stuehr, D.K. Ghosh, FT-infrared spectroscopic studies of the iron ligand CO stretch mode of iNOS oxygenase domain: effect of arginine and tetrahydrobiopterin, Biochemistry 39 (2000) 10163–10171.
[47] H.M. Abu-Soud, C. Wu, D.K. Ghosh, D.J. Stuehr, Stopped-flow analysis of CO and NO binding to inducible nitric oxide synthase, Biochemistry 37 (1998) 3777–3786.
[48] J. Wang, D.J. Stuehr, D.L. Rousseau, Tetrahydrobiopterin-deficient nitric-oxide synthase has a modified heme environment and forms a cytochrome P-420 analogue, Biochemistry 34 (1995) 7080–7087.
[49] D.W. Nebert, D.R. Nelson, M.J. Coon, R.W. Estabrook, R. Feyereisen, Y. Fujii-Kuriyama, F.J. Gonzalez, F.P. Guengerich, I.C. Gunsalus, E.F. Johnson, et al., The P450 superfamily: update on new sequences, gene mapping, and recommended nomenclature, DNA Cell Biol. 10 (1991) 1–14.
[50] M. Sono, D.J. Stuehr, M. Ikeda-Saito, J.H. Dawson, Identification of nitric oxide synthase as a thiolate-ligand heme protein using magnetic circular dichroism spectroscopy: comparison with cytochrome P-450-cam and chloroperoxidase, J. Biol. Chem. 270 (1995) 19943–19948.
[51] J.B. Schenkman, H. Remmer, R.W. Estabrook, Spectral studies of drug interaction with hepatic microsomal cytochrome, Mol. Pharmcol. 3 (1967) 113–123.
[52] T.D. Rogerson, C.F. Wilkinson, K. Hetarski, Steric factors in the inhibitory interaction of imidazoles with microsomal enzymes, Biochem. Pharmacol. 26 (1977) 1039–1042.
[53] J.B. Schenkman, S.G. Sligar, D.L. Cinti, Substrate interaction with cytochrome P-450, Pharmacol. Ther. 12 (1981) 43–71.
[54] R.A. Swanson, K.M. Dus, Specific covalent labeling of cytochrome P-450CAM with 1-(4-azidophenyl) imidazole, an inhibitor-derived photoaffinity probe for P-450 heme proteins, J. Biol. Chem. 254 (1979) 7238–7246.
[55] G.A. Roberts, A. Celik, D.J.B. Hunter, T.W.B. Ost, J.H. White, S.K. Chapman, N.J. Turner, S.L. Flitsch, A self-sufficent cytochrome P450 with a primary structural organization that includes a flavin domain and a [2Fe2S] redox center, J. Am. Chem. Soc. 278 (2003) 48914–48920.
[56] A.W. Munro, D.G. Leys, K.J. McLean, K.R. Marshall, T.W. Ost, S. Daff, C.S. Miles, S.K. Chapman, D.A. Lysek, C.C. Moser, C.C. Page, P.L. Dutton, P450 BM3: the very model of a modern flavocytochrome, Trends Biochem. Sci. 27 (2002) 250–257.
[57] R. Bhatnagar, N. Ahuja, R. Goila, S. Khetarpal, S.M. Waheed, P. Gupta, Activation of phospholipase C and protein kinase C is required for expression of anthrax lethal toxin cytotoxicity in J774A. 1 cells, Cell. Signal. 11 (1999) 111–118.
[58] R. Bhatnagar, S. Batra, Anthrax toxin, Crit. Rev. Microbiol. 27 (2001) 167–200.
[59] N. Ahuja, P. Kumar, R. Bhatnagar, Adenylate cyclase toxins, Crit. Rev. Microbiol. 30 (2004) 187–196.
[60] W. Siess, E.G. Lapetina, Functional relationship between cyclic AMP-dependent protein phosphorylation and platelet inhibition, Biochem. J. 271 (1990) 815–819.
[61] D.H. Maurice, R.J. Haslam, Molecular basis of the synergistic inhibition of platelet function by nitrovasodilators and activators of adenylate cyclase: inhibition of cyclic AMP breakdown by cyclic GMP, Mol. Pharmacol. 37 (1990) 671–681.
[62] X. Zhang, T.H. Hintze, cAMP signal transduction cascade, a novel pathway for the regulation of endothelial nitric oxide production in coronary blood vessels, Arterioscl. Thromb. Vasc. Biol. 21 (2001) 797–803.